



A novel method for gamma spectrum analysis of low-level and intermediate-level radioactive waste

Hui Yang¹ · Xin-Yu Zhang¹ · Wei-Guo Gu¹ · Bing Dong¹ · Xue-Zhi Jiang¹ · Wen-Tao Zhou¹ · De-Zhong Wang¹

Received: 20 December 2022 / Revised: 16 March 2023 / Accepted: 2 April 2023 / Published online: 21 June 2023

© The Author(s), under exclusive licence to China Science Publishing & Media Ltd. (Science Press), Shanghai Institute of Applied Physics, the Chinese Academy of Sciences, Chinese Nuclear Society 2023

Abstract

The uncertainty of nuclide libraries in the analysis of the gamma spectra of low- and intermediate-level radioactive waste (LILW) using existing methods produces unstable results. To address this problem, a novel spectral analysis method is proposed in this study. In this method, overlapping peaks are located using a continuous wavelet transform. An improved quadratic convolution method is proposed to calculate the widths of the peaks and establish a fourth-order filter model to estimate the Compton edge baseline with the overlapping peaks. Combined with the adaptive sensitive nonlinear iterative peak, this method can effectively subtracts the background. Finally, a function describing the peak shape as a filter is used to deconvolve the energy spectrum to achieve accurate qualitative and quantitative analyses of the nuclide without the aid of a nuclide library. Gamma spectrum acquisition experiments for standard point sources of Cs-137 and Eu-152, a segmented gamma scanning experiment for a 200 L standard drum, and a Monte Carlo simulation experiment for triple overlapping peaks using the closest energy of three typical LILW nuclides (Sb-125, Sb-124, and Cs-134) are conducted. The results of the experiments indicate that (1) the novel method and gamma vision (GV) with an accurate nuclide library have the same spectral analysis capability, and the peak area calculation error is less than 4%; (2) compared with the GV, the analysis results of the novel method are more stable; (3) the novel method can be applied to the activity measurement of LILW, and the error of the activity reconstruction at the equivalent radius is 2.4%; and (4) The proposed novel method can quantitatively analyze all nuclides in LILW without a nuclide library. This novel method can improve the accuracy and precision of LILW measurements, provide key technical support for the reasonable disposal of LILW, and ensure the safety of humans and the environment.

Keywords HPGe detector · Low-level and intermediate-level radioactive waste · Gamma spectrum analysis method · Deconvolution method · Continuous wavelet transform

1 Introduction

A 1000 MWe nuclear power unit will produce approximately 13,000 m³ of low-level and intermediate-level radioactive waste (LILW) [1] after 60 years of operation. After solidification or compression, this waste is prepared in 200 L and 400 L drums [2], with a total volume of approximately 3000 m³. An International Atomic Energy Agency (IAEA) technical report [3] stated that to ensure safety within the entire LILW management life cycle, the LILW must be characterized. At the same time, according to the IAEA safety standard [1], the disposal depths of LILW for different activity ranges differ, and thus quantitative analysis of LILW is necessary. Because destructive methods and time-consuming drilling are necessary to reopen a container [4],

This work was supported by the National Natural Science Foundation of China (Nos. 12205190 and 11805121) and the Science and Technology Commission of Shanghai Municipality (No. 21ZR1435400).

✉ Wen-Tao Zhou
zhwentao@sjtu.edu.cn

✉ De-Zhong Wang
dzwang@sjtu.edu.cn

¹ School of Nuclear Science and Engineering, Shanghai Jiao Tong University, Shanghai 200240, China

a nondestructive assay (NDA) is generally the best choice. Some important LILW nuclides include alpha-emitting nuclides (most actinides and transuranic nuclides) and beta-emitting nuclides (C-14, Ni-63), which cannot be used for NDA. Thus, these nuclides are called difficult-to-measure (DTM). According to the International Organization for Standardization [5], by performing gamma scanning on easy-to-measure nuclides (also called key nuclides) such as Cs-137 and Co-60, it is possible to establish a scaling factor between key nuclides and DTM and calculate the activity of the DTM. Therefore, gamma-ray scanning is required to characterize LILW.

According to the American Society for Testing and Materials (ASTM) Standard Guide [6], NDA methods include segmented gamma scanning (SGS) [7] and tomographic gamma scanning (TGS). TGS is particularly well-suited for items with heterogeneous matrix materials and non-uniform radioisotope distributions. Some studies have been conducted on SGS and TGS [8–18]. For both SGS and TGS, it is necessary to use gamma ray spectroscopy to conduct qualitative and quantitative analyses of the LILW gamma spectrum. Owing to the diverse range of nuclides in LILW and the variations between waste streams [19, 20], identifying nuclides can be challenging. Therefore, high-resolution high purity germanium (HPGe) gamma ray spectrometry is the optimal method for LILW measurement [21–25].

The spectrum measured by an HPGe detector must be analyzed to obtain the counts of gamma rays with different energies. The main steps of the spectrum analysis method [26] include smoothing, background subtraction [27], peak searching, and calculation of the peak area. Nuclide identification relies on the process of peak searching. Currently, the most mature peak-searching method is the derivative method proposed by Mariscotti [28]. GammaVision (GV) [29] and Genie 2000 [30] have adopted this method. Because of the limited peak-searching ability of the derivative method, it is necessary to establish a nuclide library to assist in identifying overlapping peaks composed of two full-energy peaks that are very close to each other. This method assumes that all gamma rays in the nuclide library are present in the spectrum, and thus it attempts to fit the peaks for every gamma energy listed in the library. Therefore, for the same peak, different results are often obtained with different nuclide libraries. For example, common LILW nuclides include Cs-137 emitting 662 keV and Ag-110 m emitting 658 keV. The nuclide composition of the LILW before measurement is not accurately known. For the same full-energy peak of 662 keV, if only 662 keV is defined in the nuclide library, the quantitative analysis result is accurate. However, if both 658 and 662 keV are provided in the nuclide library, the report will provide a full-energy peak count of 658 keV. This results in misidentification of the nuclide. At the same time, the calculated 662 keV peak area decreases, resulting

in inaccurate activity calculations, which is a potential safety hazard for the disposal of LILW. The IAEA report [29] also noted that this method requires the availability of good nuclear data libraries. Other peak-finding methods include the IF function method [31], zero-area fold-in method [32], Gaussian product function method [33], covariance method [34], continuous wavelet transform (CWT) method [35], and neural network method [36]. Compared with the derivative method, these methods are an improvement; however, they still require auxiliary identification of the nuclide library.

In this study, to solve the problem of uncertainty in the nuclide library causing instability in the analysis results for LILW spectra, a novel spectrum analysis method is proposed to reduce this uncertainty and improve accuracy. For each step in the spectral analysis process, the overlapping peak decomposition process does not rely on the assistance of the nuclide library. This study improves the accuracy of LILW measurements and provides key technical support for the safe disposal of LILW.

2 Materials and methods

2.1 Analysis method

2.1.1 Traditional spectral analysis method

In traditional spectral analysis methods, there are problems with each of the basic steps. When smoothing the spectrum according to a five-point smoothing algorithm [37], the processing causes the maximum value of the peak to decrease each time, and the counts on both sides of the bottom of the peak increase. Thus, the calculation of the peak area is inaccurate. At the same time, it is difficult to identify the nuclide because of the changes in the peak shape.

According to the GammaVision user manual [37], background subtraction methods include the straight-line, stepped, and parabolic background methods [38]. These methods provide only rough approximations of the background, thereby increasing the peak area calculation error. At the same time, Miroslav [39] showed that the parabolic background had very poor robustness [38].

The peak search method was proposed by Mariscotti [28]. This method has a limited ability to separate overlapping peaks [32], resulting in inaccurate nuclide identification; furthermore, it is highly susceptible to noise. Thus, it is necessary to smooth the spectrum multiple times before searching for the peak, which leads to changes in the peak shape and increases the error in the peak area calculation.

The final step is the quantitative analysis of overlapping peaks. In traditional methods, a preliminary library-based peak search of the spectrum is performed. The analysis assumes that all of the gamma rays listed in the library

are present in the spectrum; therefore, an attempt is made to fit a peak at every gamma energy listed in the library. Therefore, as reported in Ref. [40], if the nuclide library is inaccurate, it will increase the error in the spectral analysis results.

2.1.2 Spectral analysis method proposed in this study

According to Knoll [41] and the IEC international standard [42], for a single overlapping peak composed of multiple full-energy peaks with similar energies, the only method to conduct an analysis is through deconvolution. The deconvolution method can be used to establish the relationship between the incident gamma ray spectrum and the energy deposition spectrum using the response function of the detector, as follows [43]:

$$y(t) = \int_{-\infty}^{\infty} x(\tau)h(t - \tau)d\tau + n(t), \tag{1}$$

where $x(\tau)$ is the incident spectrum, $y(t)$ is the energy deposition spectrum, $h(t)$ is the response function, t is the channel, and $n(t)$ is the system noise. Therefore, the core concept of this method is to use the peak shape function, $h(t)$, as a filter, and then to obtain the incident spectrum through deconvolution to realize the decomposition of overlapping peaks.

For $h(t)$, because of the different attenuations of the medium during gamma ray measurement under different conditions, it is difficult to establish the full-spectrum response under such complex and variable conditions through experiments or Monte Carlo simulations. Because the full-energy peak areas of the different nuclides are regarded as regions of interest in this study, it was only necessary to determine the full-energy peak response. The full-energy peak of the HPGe detector can be represented by a Gaussian function. Theoretically, according to the full width at half maximum (FWHM) of the full-energy peak, the response can then be obtained via calculations. Therefore, before the spectral analysis, an experimental method was used to calibrate the FWHM. The FWHM is different for different energies; therefore, the following equation is used for parameter fitting [44]:

$$FWHM = a + b\sqrt{E + c \times E^2}, \tag{2}$$

where E is the gamma energy. The HPGe detector used in this study was calibrated using the experimental method. When the energy unit is MeV, the values of a , b , and c are 0.00068, 0.00062, and 1.07, respectively.

For a discrete system, $h(t)$ can be expressed as a matrix [45]:

$$\begin{bmatrix} h_1(1) & 0 & 0 & \vdots & 0 \\ h_1(2) & h_2(1) & 0 & \vdots & \vdots \\ h_1(3) & h_2(2) & h_3(1) & \vdots & \vdots \\ \vdots & h_2(3) & h_3(2) & \vdots & 0 \\ h_1(A) & \vdots & h_3(3) & \vdots & h_m(1) \\ 0 & h_2(B) & \vdots & \vdots & h_m(2) \\ 0 & 0 & h_3(C) & \vdots & \vdots \\ \vdots & \vdots & \vdots & \vdots & h_m(N - 1) \\ 0 & 0 & 0 & \vdots & h_m(N) \end{bmatrix} \tag{3}$$

where each column of the matrix is the probability density function of the full-energy peak response, and the subscripts of h indicate the gamma rays emitted from that channel. Because the FWHMs of the different full-energy peaks are different, the values of a–n represent the peak widths of different full-energy peaks.

The solution to Eq. (1) is an ill-posed problem. According to Miroslav [46], iterative regularization has strong positive constraints and noise-suppression capabilities. Currently, the most effective method for gamma spectrum analysis is the boosted traditional iterative algorithm [47]. In this study, a boosted maximum-likelihood expectation–maximization algorithm [48] was used.

Through this deconvolution process, the deposition spectrum of gamma rays with different energies can be converted into the incident δ function spectrum; thus, nuclide identification can be easily performed. Its height corresponds to the area of the full-energy peak. However, in the realization of this process, another problem must be solved, i.e., the background must be effectively subtracted from the original spectrum to obtain a “net spectrum” containing only the full-energy peak.

Background subtraction methods include the linear method [30], approximate physical models for the background, the polynomial method [49], digital filtering [50], peak clipping [38], fast Fourier transform [51], and the sensitive nonlinear iterative peak (SNIP) method [52]. Among these methods, the most effective background subtraction method is the improved SNIP method, i.e., adaptive SNIP [39].

The basic concept of the adaptive SNIP method is to divide the energy spectrum into two regions: the region where the peak is located, and the region where there is no peak. For the peak area, the SNIP filter is used for background subtraction, and for the non-peak area, all of the gamma counts are regarded as the background. Therefore, the problem is to determine how to calculate the peak position, peak width, and selection of the clipping filter.

This study proposes a calculation method for peak position identification based on CWT. The wavelet transform of a signal x is given as follows [35]:

$$T(E, s) = \int_{-\infty}^{\infty} x(t)\psi_{E,s}^*(t)dt, \tag{4}$$

where E is the gamma ray energy, s is the scale of the wavelet, $\psi_{E,s}(t)$ is the mother wavelet, and $T(E, s)$ is the scalogram. The scale s represents the stretching and shrinking of the wavelet, as expressed in the following equation [53]:

$$\psi_{E,s}(t) = \frac{1}{\sqrt{s}}\psi\left(\frac{t-E}{s}\right). \tag{5}$$

The correct choice of wavelet is the key to obtaining the results of the spectrum analysis. As the full-energy peak of the spectrum is a Gaussian function, a Mexican hat wavelet (Mexh) is selected because its shape is similar to that of a Gaussian peak. The definition of Mexh is given as follows [54]:

$$\psi_{\text{Mexh}}(t) = \frac{2}{\sqrt{3\sigma}\pi^{1/4}}\left(1 - \left(\frac{t}{\sigma}\right)^2\right)e^{-\frac{t^2}{2\sigma^2}}. \tag{6}$$

By analyzing the scalogram, the position information of the peak can be obtained. The next step is to calculate the widths of the peaks based on their positions.

The peak width can be obtained directly from the scalogram obtained with Eq. (4), but because the peak widths of different scales are different, this method has large errors [55]. The peak width can be calculated using a Gaussian product function [33], but it is highly susceptible to noise interference. The width can also be determined from the shapes of the peaks using function fitting [56]. This approach is also difficult to use because the number of singlets comprising the overlapping peaks is unknown. In Refs [55] and [56], a method for calculating the peak width based on the second convolution of the Gaussian first derivative was proposed.

The expression for the full-energy peak is as follows [57]:

$$G(x) = A\exp\left(-\frac{(x-a)^2}{2\sigma^2}\right), \tag{7}$$

where x is the channel, A is the count of the full-energy peak maxima, a is the peak position, and σ is the standard deviation of the full-energy peak.

The calculation result for the second convolution of the Gaussian first-order derivative of Eq. (7) is expressed as follows [54]:

$$C(x) = \frac{2\pi\delta^2\sigma((x-a)^2 - \sigma^2 - 2\delta^2)}{(\sigma^2 + 2\delta^2)^{5/2}}\exp\left(-\frac{(x-a)^2}{2(\sigma^2 + 2\delta^2)}\right), \tag{8}$$

where δ represents the width of the filter.

Using Eq. (8), the crossing point of the zero value can be determined as follows [54]:

$$\sigma = \sqrt{(x_0 - a)^2 - 2\delta^2}, \tag{9}$$

where a is the peak position calculated with the CWT, and x_0 is the intersection point with the x -axis. Then, $[a - 3\sigma, a + 3\sigma]$ is the width of the area in which the peak is located.

However, other studies have shown that this method is not suitable for calculating overlapping peak widths that contain too many full-energy peaks [39]. Therefore, in this study, we propose an improved method.

For Eq. (8), the calculation of the width of the peak requires the determination of the parameter σ , while the parameter δ is also unknown. Thus, a method is required to determine parameters σ and δ . For $C(x)$ in Eq. (8), when $\frac{dC(x)}{d\delta} = 0$, it is easy to obtain $\delta = \sigma$, and this is the maximum value of $C(x)$. Therefore, the absolute value of $C(x)$ is first computed, and then a matrix $M(x, \delta)$ is built. Its horizontal axis, x , represents different channels. The vertical axis of $M(x, \delta)$ indicates that for each x , the value of $C(x)$ is calculated for different δ . In other words, for each x , the calculation is performed by traversing the possible values of δ (for example, 0.1–100) and then calculating a $C(x)$ curve. This is carried out because at the maximum value of $C(x)$, $\delta = \sigma$, the value of σ can be obtained based on the value of δ , and the peak width can then be effectively calculated. In the application, the horizontal axis, x , only considers the peak position information calculated based on the CWT.

Next, the background of the peak area must be removed. For the SNIP method, first, to compress the dynamic range of each channel count in the spectrum to speed up the iteration, a linear least-squares operator is applied to the spectrum data [52]:

$$v(i) = \log\left\{\log\left[\sqrt{y(i)+1} + 1\right] + 1\right\}, \tag{10}$$

where i is the channel, $y(i)$ is the count of each channel, and $v(i)$ is the working vector.

For the count $v(i)$ of each channel, the parameter m is selected, and then $w = 2m + 1$. The following equation is then used to iteratively calculate $v_1(i), v_2(i), \dots, v_m(i)$ [52]:

$$v_p(i) := \min\left\{v_{p-1}(i), \frac{1}{2}[v_{p-1}(i+p) + v_{p-1}(i-p)]\right\}, \tag{11}$$

where $p \in [1, m]$, $i \in [p, size_y]$, and $size_y$ is the size of spectrum y . For parameter w , when the value of w is too small, the background estimate will be too large, and the net peak area will be too small. If the value of w is too large, the background estimate will be small, and the net peak area will be large. Theoretically, the background should be removed as much as possible while preserving the net peak areas.

The real width of an object (peak, doublet, or multiplet) that should be preserved is the best value of w [58]. In the proposed method, the width of each peak is calculated based on the second convolution of the Gaussian first derivative, and the clipping width, w , of each peak is obtained; that is, the value of w is dynamic. Then, the SNIP algorithm is utilized. Finally, a linear least-squares inverse operator operation is performed on $v_m(i)$ to obtain the background spectrum.

For the adaptive SNIP [39], the spectrum is divided into two areas: the non-peak and peak areas. In the non-peak region, all of the gamma counts are the background. In the peak region, the background is subtracted using the traditional SNIP method. Equation (11) represents a second-order filter that can effectively remove the linear background. To solve the problem of the inability to subtract the background at the Compton edge for the full-energy peak as described in Sect. 2.1.1, a novel method is proposed.

Because the Compton edge can be approximated by a cubic function to some extent, and a cubic function can be removed by a fourth-order clipping filter, a fourth-order clipping filter is proposed for background subtraction in the peak area. The parameters of the equation were derived from Pascal's triangle [59] formula. The fourth-order clipping filter is defined as follows:

$$\begin{cases} V_1 = v_{p-1}(i) \\ V_2 = \frac{v_{p-1}(i-p) + v_{p-1}(i+p)}{2} \\ V_3 = \frac{-v_{p-1}(i-p) + 4v_{p-1}(i - \frac{p}{2}) + 4v_{p-1}(i + \frac{p}{2}) - v_{p-1}(i+p)}{6} \\ v(i) = \min[V_1, \max(V_2, V_3)] \end{cases}, \quad (12)$$

where the definitions of these parameters are identical to those in Eq. (11).

Through the peak searching and peak width calculations described above, the spectrum can be divided into peak and non-peak areas, which are combined with a fourth-order clipping filter in the peak area. Thus, effective subtraction of the background is realized and the net spectrum is obtained.

During the smoothing process in the traditional method, the peak count will decrease. This study uses a low-pass

filter [52] to smooth the spectrum and effectively solve this problem.

2.2 Experimental condition

2.2.1 Experimental configuration

The HPGe detector was an Integrated Cryocooling System produced by ORTEC. Its relative efficiency at 1.33 MeV is 30%. The detector crystal has a diameter of 51.8 mm and length of 60.9 mm. The cold finger has a diameter of 8.7 mm and a length of 38.2 mm. The dead layer at the front end of the crystal has a thickness of 0.03 mm. The DSPEC-50 multi-channel analyzer was manufactured by ORTEC.

GV 6.08 spectral analysis software was used. The analysis parameters of GV included the calibration (.CLB) file, peak background correction (.PBC) file, and nuclide library (.LIB) file; the analysis program was WAN32. The standard area of the peak was calculated by selecting the region of interest (ROI) in the GV; the peak width was three FWHM.

The experiments were conducted using the Tomographic Gamma System (SJTU-TGS), which was independently developed by Shanghai Jiao Tong University, as shown in Fig. 1a. The detector was equipped with a lead collimator (liftable). The exterior dimensions of the collimator and collimation window were 25 cm (L) \times 36 cm (W) \times 40 cm (H) and 9 cm (L) \times 20 cm (W) \times 25 cm (H), respectively, and the thickness of the lead was 8 cm. The distance between the detector surface and drum center was 74 cm. The system had a liftable transmission source storage device. The waste drum could be moved and rotated. Therefore, the measurement system had detection functions of SGS and TGS and could also meet the requirements of 200 L and 400 L waste drums at the same time.

2.2.2 Source test conditions

To verify the accuracy of the spectral analysis of the different nuclides, the radioactive sources used were standard point sources: monoenergetic gamma ray nuclide Cs-137

Fig. 1 (Color online) **a** SJTU-TGS System; **b** Canberra SGS System



[60] (7.86×10^5 Bq) and multi-energy gamma-ray nuclide Eu-152 [61] (2.74×10^6 Bq).

To obtain the spectrum of the radioactive source attenuated by different densities, the radioactive source was placed in a 200 L drum filled with different materials for measurement. The materials used in the drum were air (the empty drum), water (1 g/cm^3), and sand (1.6 g/cm^3).

To explore the influence of different nuclide libraries on the GV analysis results, multiple verification experiments were conducted on 200 L drums. The radioactive source, Cs-137, was placed at different positions in the drum, as shown in Fig. 2, and the drum was not filled with material. The time for each measurement was 10 min.

2.2.3 SGS experiment

The purpose of spectral analysis is to measure the activity of LILW. Therefore, a 200 L standard drum was employed. The material in the drum was water. Cs-137 was placed at radii of 0, 6.25, 11.25, 16.25, 21.25, and 26.25 cm, and the height was 42.5 cm (half the height of the drum). SGS [7, 16] was used for activity reconstruction based on the SJTU-TGS system.

The same standard drum was used for activity reconstruction with the Canberra SGS System [25], as shown in Fig. 1b. The aim of this study was to compare and analyze the activity measurement results of the two systems. The spectroscopy software in the Canberra SGS System is Genie 2000 [30], and the software for measurement activity is NDA2000 [62]. To control for the variables, the SJTU-TGS System adopts the SGS method described in NDA2000 (refer to Refs [7], and [61]). The efficiency calibration method of the SJTU-TGS system adopts the method described by Qian [12], which meets the ASTM standards [63]. Because the material was water, this was an easy task for efficient calibration. It was assumed that any calibration method would provide relatively consistent results. During the gamma scanning, the drum was vertically divided into eight layers, and the lifetime of each layer was 1 min.

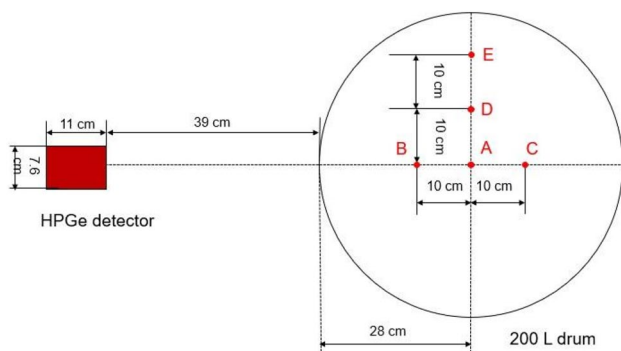


Fig. 2 Schematic diagram of the locations of the radioactive source

Considering the dead time and moving time of the detector, the measurement time for a drum was approximately 10 min, which was within the measurement time range for 200 L drums in nuclear power plants. The only difference is that the SJTU-TGS System adopted the novel spectral analysis method proposed in this study. For the Canberra SGS System according to Genie 2000, its method was very close to GV, and thus it represented the traditional spectrum analysis method.

3 Experiments and discussion

The verification experiments for the spectral analysis method included the following parts: a preliminary verification experiment for a single nuclide, instability experiments for the nuclide library, activity measurement comparison experiments for the standard drum, and overlapping peak simulation spectrum experiments.

3.1 Preliminary verification experiment for a single nuclide

3.1.1 Spectra of monoenergetic gamma ray nuclides

The original spectra of the Cs-137 nuclide without attenuation and those attenuated by water and sand are shown in Fig. 3a; the normalized spectra are shown in Fig. 3b. The Compton plateau in the attenuated spectrum is significantly higher than that in the unattenuated spectrum. Three spectra were analyzed using the proposed method. For comparison, GV was used to establish an accurate nuclide library and the nuclide analysis results were obtained. The spectral analysis results obtained using different methods are shown in Fig. 4, and the quantitative results are presented in Table 1.

As shown in Fig. 4, through the deconvolution process, the proposed method converted the number of full-energy peak channels into one channel, making it very easy to identify nuclides. The results in Table 1 indicate that because of the simple task of single-peak nuclide identification, the results were similar to those of GV, and the errors for both methods were less than 3%.

3.1.2 Spectra of multi-energy gamma ray nuclides

Because the nuclides in LILW generally emit multi-energy gamma rays, the Eu-152 spectrum was used for analysis and verification. The original spectrum of Eu-152 is shown in Fig. 5a. Gamma rays for eleven energies with the largest peak areas were selected for analysis. Because the energy resolution of HPGe is very good, the overall spectral lines appeared very clear. However, in the zoomed-in details, such as the 778.90 keV full-energy peak shown in Fig. 5a, the

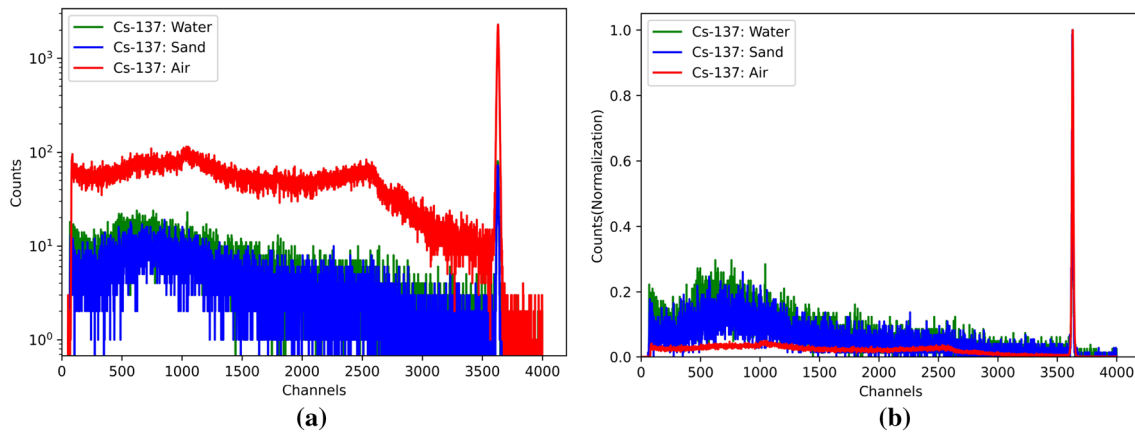


Fig. 3 (Color online) **a** Original spectra of Cs-137 attenuated by different materials; **b** Normalized spectra of Cs-137 attenuated by different materials

peak width was approximately 20 channels. The results of the spectral analysis using the novel method are shown in Fig. 5b. It can be observed that the gamma rays occupied only one channel, as seen in the zoomed-in details of the 778.90 keV full-energy peak. Thus, the accurate identification of nuclides could be realized.

The results of the quantitative analysis of the novel method and GV are compared in Table 2. For the calculation errors of the full-energy peaks with different energies, the proposed method was more accurate, with a maximum error of 8.28%, whereas the maximum error of GV was 18.40%. This is because in the energy spectrum analysis process of GV, spectral smoothing is first performed, leading to some changes in the peak shape, and the peak area is calculated by fitting these peak shapes. Therefore for peaks with large statistical fluctuations, particularly those with relatively small peak areas, significant errors can be introduced during the smoothing and fitting processes. However, in the novel method, the full-energy peak is directly used to calculate the peak area during the process of deconvolution; thus, there is almost no significant deviation in the calculation of the peak area. From the perspective of the mean error (average error from all the peaks), GV has an error of 5.43%, whereas the novel method has an error of 3.89%.

3.2 Nuclide library instability experiments

These GV analysis results were based on an accurate nuclide library. However, in practical applications, it is generally difficult to make an accurate judgment regarding the suitability of the nuclide library. Therefore, for the same Cs-137 (662 keV) spectrum attenuated by sand, different nuclide libraries were used to analyze the GV results. Analytical results are also provided for this novel method, which does not require the establishment of a nuclide library. Because

Ag-110 m is the most common corrosion activation product in LILW and its gamma emission of 658 keV is close to that of Cs-137, the nuclide library settings were as follows: Cs-137, Cs-137 + Ag-110 m, and Ag-110 m. The GV analysis results are presented in Fig. 6 and Table 3.

As shown in Fig. 6, for the Cs-137 spectrum, if only Cs-137 was included in the nuclide library, the analysis result was accurate and the peak area error was only 2.7%. However, when Ag-110 m was added to the nuclide library, a peak area of Ag-110 m was obtained based on the spectral analysis mechanism; in other words, Gaussian functions with energies of 658 and 662 keV fit the full-energy peak of Cs-137. Therefore, the areas of the full-energy peaks of the two energies could be obtained, and thus the error of the peak area of Cs-137 increased to 32.3%. In the absence of Cs-137 in the nuclide library, the result did not provide a count of Cs-137; in other words, different nuclide libraries yielded completely different analytical results. By assuming the presence of a peak a priori, GV was “forced” to calculate the properties of the peak. This finding was consistent with the conclusions of Santoro [40]. Because the novel method does not require a nuclide library, the error in the analysis result was stable at 0.4%.

To further explore the influence of different nuclide libraries on the GV analysis results, verification experiments were carried out on 200 L drums, as shown in Fig. 2. For the nuclide library setting of the GV, in addition to Cs-137 (662 keV) and Cs-137 + Ag-110 m (662 keV + 628 keV), an artificial nuclide library was used with a composition of 662, 661, 660, 659, and 658 keV. The results of the spectral analyses with different methods are shown in Fig. 7, where the x-axis represents the identification number of the radiation source at different positions inside the 200 L drum. The analysis results of the novel method and the GV based on an accurate nuclide

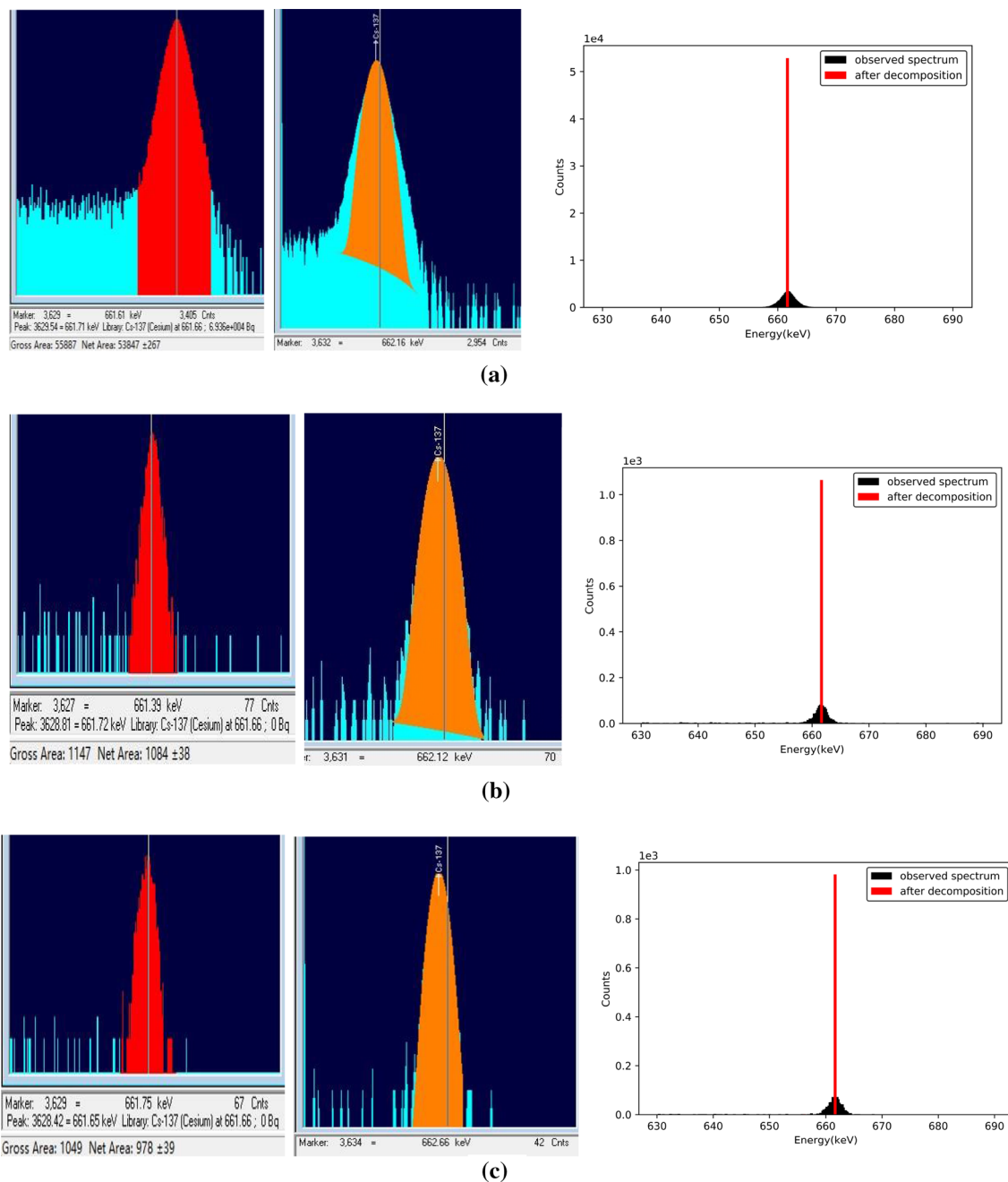


Fig. 4 (Color online) Analysis results of the Cs-137 spectrum with different methods: **a–c** spectra attenuated by different materials (air, water, and sand). Left: Standard peak area of ROI; middle: GV; right: Novel method

library were similar. The average relative error of the novel method was 3.3%, and that of GV was 3.4%. However, when the GV nuclide library consisted of two gamma energies, the 662 keV peak was fitted into two peaks, and thus the average error of the 662 keV peak was 38.3%. When the nuclide library consisted of five gamma energies, the 662 keV peak had the worst average error of 48.3% because 662 keV was “split” into five overlapping peaks.

3.3 Activity reconstruction for a 200 L drum

For the 200 L standard drum, the SGS activity reconstruction results using the SJTU-TGS and Canberra SGS systems are shown in Fig. 8.

For the two systems, except for the spectral analysis method, the other methods are basically the same. Therefore, theoretically, the activity reconstruction

Table 1 Analysis results for the Cs-137 spectrum attenuated by different materials with different methods

Material	Method	Standard peak area of ROI	Calculated peak area	Error (%)
Air	GV	54,226	55,676	2.4
	Novel method		52,895	-2.71
Water	GV	1084	1091	0.65
	Novel method		1065	-1.75
Sand	GV	978	1004	2.66
	Novel method		982	0.41

error primarily reflects the error of the spectral analysis method. As shown in Fig. 8, when the radius was relatively small, the measured value was low. As the radius increased, the measured value also increased. Because

the SGS method was aimed at LILW in which the matrix and nuclides are uniformly distributed, the object of efficiency calibration was a uniform volume source. The Cs-137 source at different positions in this experiment was categorized as a situation in which the distribution of nuclides was extremely uneven, which does not satisfy the basic conditions of SGS. Thus, relatively large measurement errors inevitably occurred. For non-uniform cases, SGS can reach a maximum measurement error of more than 500% [64]. Therefore, when the radius of the source is small, the value of the efficiency calibration is too large and the measured value is too small. In theory, for the SGS method, there is generally an equivalent radius at the position of 0.7–0.8 *R* (*R* is the radius of the drum) [15, 16], and the actual efficiency value at this position is close to the efficiency of the uniform source value. As a result, better measurement results can theoretically be

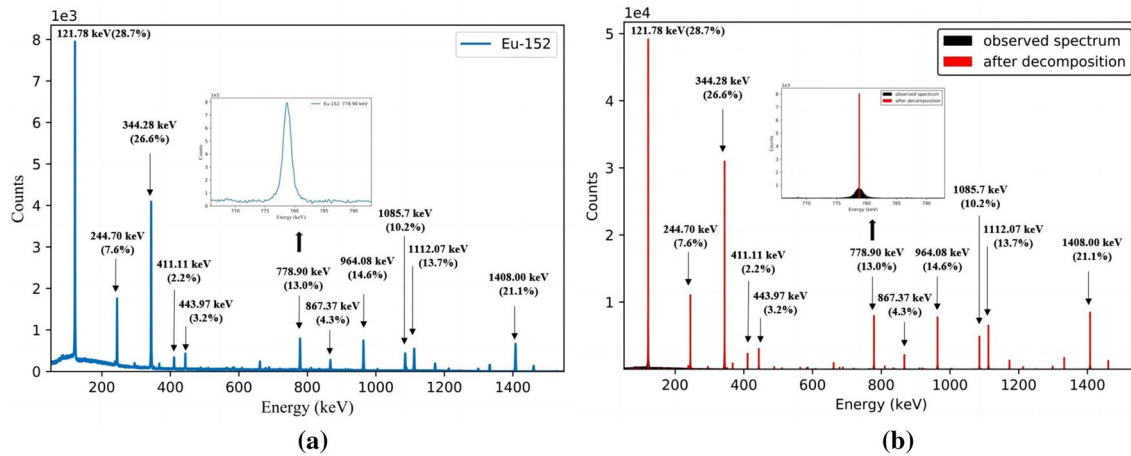


Fig. 5 a Original spectrum of Eu-152; b Spectrum analysis results for Eu-152 with the novel method. The percentages represent gamma ray emission probabilities

Table 2 Comparison of the spectral analysis results for Eu-152 with different methods

Energy	Standard peak area	Calculated peak area (GV)	Error (GV) (%)	Calculated peak area (novel method)	Error (novel method) (%)
121.78	47,650	48,026	0.79	49,262	3.38
244.70	10,908	10,844	-0.59	11,115	1.90
344.28	30,823	30,083	-2.40	31,042	0.71
411.11	2283	2703	18.40	2401	5.17
443.97	2873	2987	3.97	3111	8.28
778.90	7794	8057	3.37	8047	3.25
867.37	2177	2456	12.82	2214	1.70
964.08	7377	7497	1.63	7811	5.88
1085.87	4760	5235	9.98	4953	4.05
1112.07	6369	6704	5.26	6589	3.45
1408.00	8122	8163	0.50	8528	5.00
Mean error			5.43		3.89

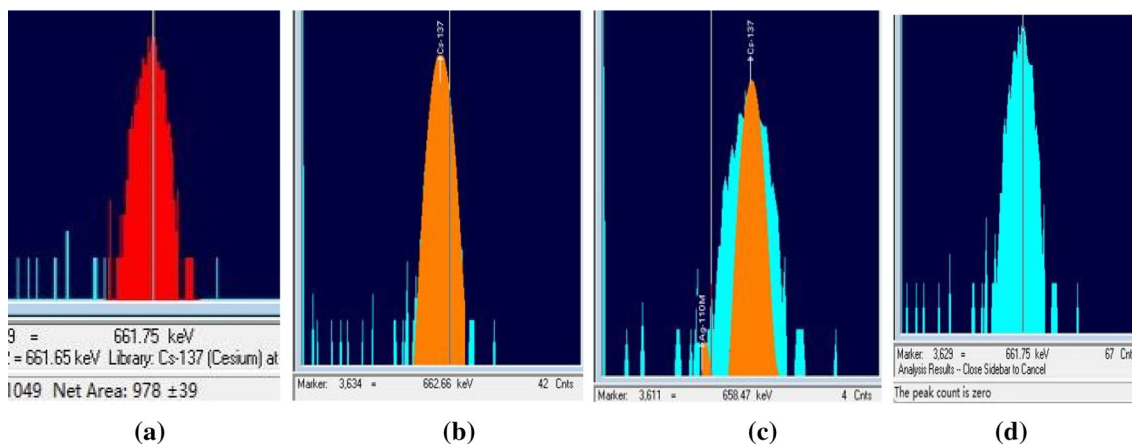


Fig. 6 (Color online) **a** Cs-137 original spectrum; **b** GV results based on the nuclide library for Cs-137; **c** GV results based on the nuclide library for Cs-137 + Ag-110 m; (d) GV results based on the nuclide library for Ag-110 m

Table 3 Comparison of spectral analysis results with different nuclide libraries

Number	Nuclide library (GV)	Standard peak area	Calculated peak area (GV)	Error (GV) (%)	Calculated peak area (novel method) (%)	Error (novel method) (%)
1	Cs-137	978	1004	2.7	982	0.4
2	Cs-137 + Ag-110 m	978	662	32.3	982	0.4
3	Ag-110 m	978	—	—	982	0.4

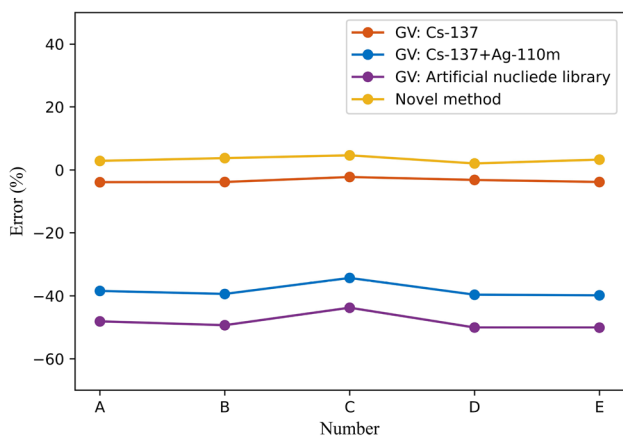


Fig. 7 (Color online) Comparison of the results of different methods

obtained. Therefore, for the SJTU-TGS System, when the radius was 21.25 cm, it was close to the equivalent radius, and the spectral analysis results were relatively accurate. Therefore, the error was only 2.4%, whereas for the Canberra SGS System, the smallest error was 12.9%. To some extent, this reflects the accuracy of the spectrum analysis.

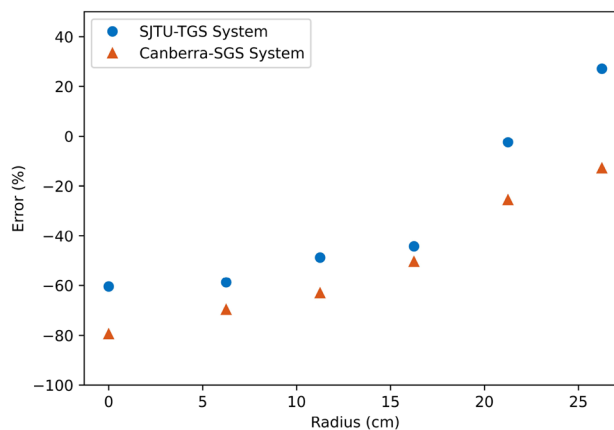


Fig. 8 Comparison of the activity reconstruction errors for 200 L drums with different systems

3.4 Analysis of overlapping peaks

3.4.1 Verification of the accuracy of the Monte Carlo simulation method

The types of nuclides in LILW are complex, and it is difficult to obtain different overlapping peaks experimentally to verify the spectral analysis method. Therefore, a Monte Carlo simulation was used in this study to simulate the process of

measuring the radioactive source with an HPGe detector. A geometric model was constructed using the Geant4 tool [65, 66]. According to the certificate of calibration (SRS number: 116230 and product code: 8403-GF-PNT) corresponding to the HPGe detector provided by ORTEC, the hybrid source (a point source in tape in a 2-inch aluminum ring) was placed horizontally 30 cm from the front end of the detector, and the detection efficiency curve was obtained experimentally. A comparison between the Monte Carlo simulation efficiency [67–70] and the experimental efficiency [71] is shown in Fig. 9a. Except for the relative error of the full-energy peak efficiency at an extremely low energy (46.52 keV), which was 9.89%, all of other calculation errors were less than 5%.

The Cs-137 spectrum experiment was conducted according to the measurement standard requirements of ANSI [72] and IEEE [73]. The collected full-energy peak count exceeded 20,000. The gamma count of the environmental background within the same measurement time was subtracted using the channel-by-channel method to obtain the net spectrum. A comparison between the normalized spectrum of the experiment and the Monte Carlo simulation is shown in Fig. 9b. In addition to certain statistical fluctuations in the experimental spectrum, the full-energy peak and Compton plateau were in good agreement, verifying the accuracy of the Monte Carlo simulations.

3.4.2 Spectral analysis of key LILW nuclide overlapping peaks

Based on the key nuclide types of the LILW provided by the Qinshan Nuclear Power Plant and through the comparison and analysis of nuclides and their characteristic energies, three nuclides with the closest characteristic energies were selected: Sb-125 (601 keV), Sb-124 (603 keV), and Cs-134 (605 keV).

Different peak area ratios were set for the compositions of the three overlapping peaks. Because the overlapping peaks are difficult to decompose, it is easier to identify the nuclide as a full-energy peak located in the middle channel of the overlapping peaks. Therefore, if the peak area at the middle energy is lower than that on both sides, thus forming a weak peak, it is easier to elucidate the performance of the spectral analysis methods. Therefore, three overlapping peaks were set with peak area ratios of 5:1:10, 10:1:20, and 20:1:40 for 601, 603, and 605 keV, respectively. For overlapping peaks with larger area ratios, because the activity calculated with this weak peak does not contribute significantly to the total activity of LILW and does not affect its final disposal, it was not necessary to continue studying these cases. At the same time, to illustrate the difficulty of identifying overlapping peaks, the CWT with the strongest performance in the traditional peak searching method was used for comparison. The results of the spectral analysis are shown in Fig. 10, and the quantitative results are summarized in Table 4.

As shown in Fig. 10a, through the precise deconvolution process, the novel method decomposed the overlapping peaks into three incident spectra whose shape was a δ function, and the positions of the three full-energy peaks were accurately identified without energy deviation. The maximum area calculation error of the strong peak was -0.28% , and the error of the weak peak was 0.48% . CWT was used to analyze the overlapping peaks, and three full-energy peaks were observed in the scalogram. However, one weak peak was located in the middle of the overlapping peaks; therefore, the weak peak was more difficult to identify. As shown in Fig. 10b, there was no energy deviation in the positioning of the three full-energy peaks. The area maximum calculation error for the strong peak was -0.28% at most, and that for the weak peak was 1.72% .

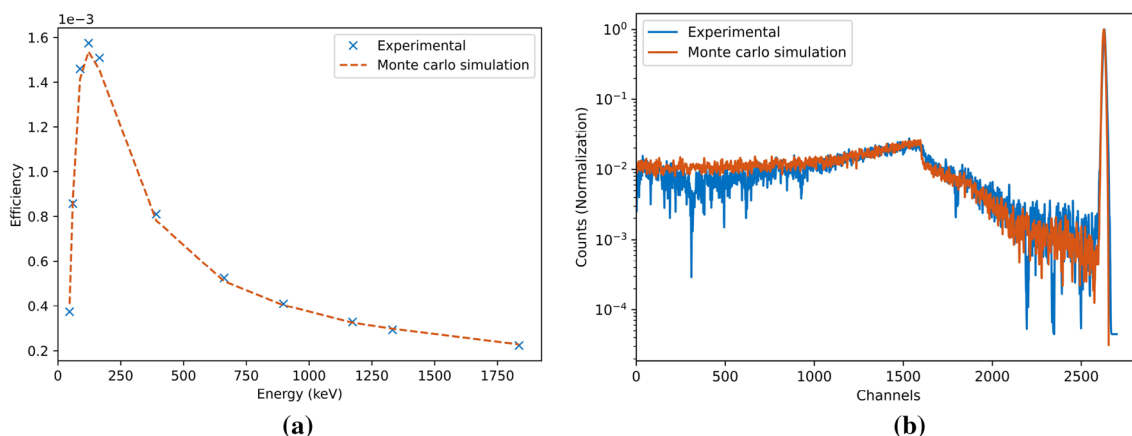


Fig. 9 (Color online) **a** Comparison between the Monte Carlo simulation and experimental efficiencies; **b** Comparison of Cs-137 spectra with different methods

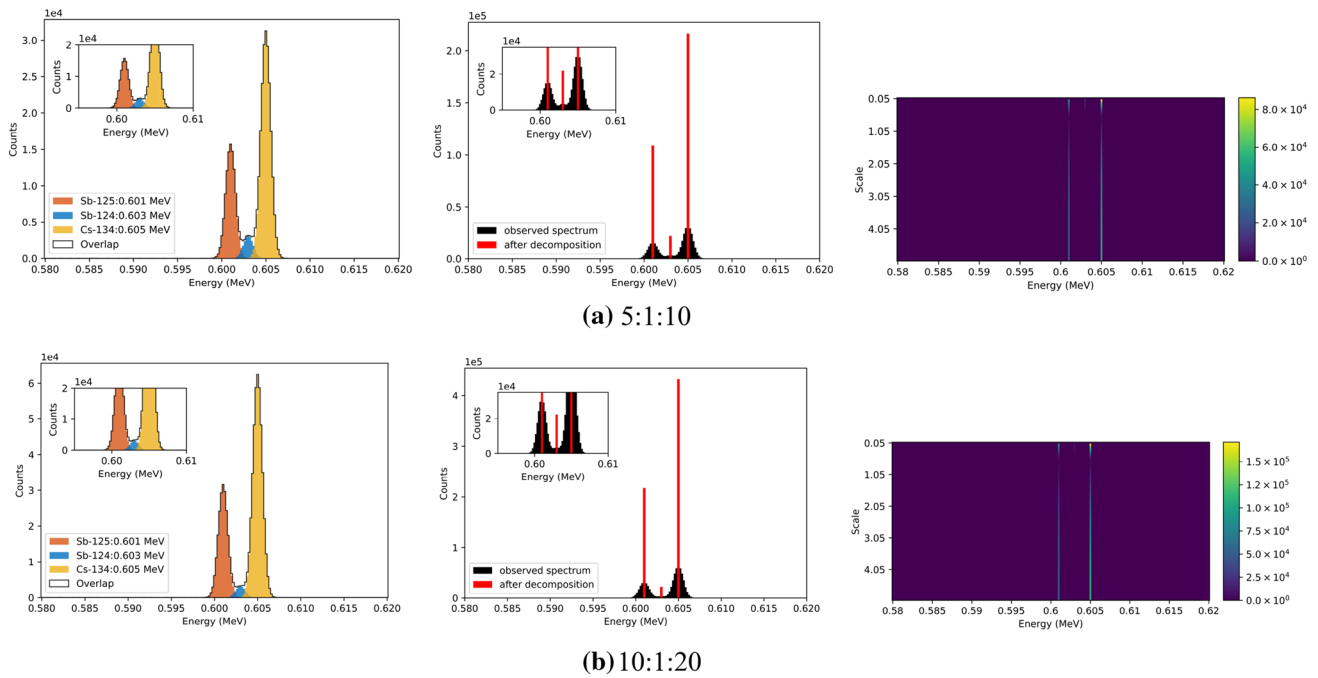


Fig. 10 (Color online) Analysis results of overlapping peaks with different peak area ratios: **a–c** represent peak area ratios of 5:1:10, 10:1:20, and 20:1:40, respectively. Left: original spectra; middle: spectral analysis results with the novel method; right: scalogram of CWT peak searching

Table 4 Spectral analysis results with different overlapping peaks

Number	True value			Calculated value		
	Nuclide	Energy (keV)	Peak area	Energy (keV)	Peak area	Peak area error (%)
(a)	Sb-125	601	109,278	601	108,969	−0.28
	Sb-124	603	21,920	603	22,026	0.48
	Cs-134	605	217,095	605	216,716	−0.17
(b)	Sb-125	601	217,958	601	217,486	−0.22
	Sb-124	603	21,920	603	22,297	1.72
	Cs-134	605	434,017	605	432,783	−0.28
(c)	Sb-125	601	438,854	601	437,810	−0.24
	Sb-124	603	21,920	603	22,653	3.34
	Cs-134	605	868,397	605	865,777	−0.30

As shown in Fig. 10c, under the condition of a peak area ratio of 20:1:40, by zooming in on the details in the original spectrum, because the area ratio of the three full-energy peaks was very different, it was determined that the 603 keV full-energy peak in the middle was completely covered by the high-energy peaks on both sides. The 603 keV full-energy peak was submerged. In the CWT scalogram, the weak peak at 603 keV could not be identified, and only two strong peaks at 601 and 605 keV could be identified. With the novel method, accurate nuclide identification could still be achieved for

overlapping peaks in such extreme cases. The largest area calculation error for the strong peak was −0.3%, whereas that for the weak peak was 3.34%.

As shown in Fig. 10, for overlapping peaks under some extreme conditions, it was difficult for CWT to achieve an accurate nuclide analysis. CWT in the novel method was used to determine the positions of the overlapping peaks and perform subsequent peak width IAEA calculations. At this point, it did not matter which nuclides constituted the overlapping peaks.

4 Conclusion

In LILW spectrum analysis using existing methods, uncertainty of the nuclide library causes instability in the analysis results and reduces the accuracy of activity reconstruction. To address this problem, this study proposes a novel spectral analysis method. Through standard source experiments, standard drum experiments, and Monte Carlo simulation experiments, the following conclusions are drawn:

1. The novel method and GV with an accurate nuclide library exhibited similar spectrum analysis capabilities, and the analysis errors were less than 3% for Cs-137 and 4% for Eu-152.
2. The novel method does not require a nuclide library, and the analysis results were more stable than those of GV, which showed significant errors and instability in peak area calculations.
3. The novel method could be applied to the activity measurement of LILW, and the reconstructed activity of Cs-137 was accurate, with an error of 2.4%, while the minimum measurement error of the Canberra system was 12.9%.
4. The novel method could quantitatively analyze all of the nuclides in LILW without a nuclide library. For overlapping peaks composed of peak area ratios of 5:1:10, 10:1:20, and 20:1:40, the nuclide could be accurately identified; the area calculation error of the strong peaks was less than 1%, and the error of the weak peaks was less than 4%.

This novel method can improve the accuracy and precision of LILW measurements, provide key technical support for the reasonable disposal of LILW, and ensure the safety of humans and the environment.

Author's contributions All authors contributed to the study conception and design. Material preparation, data collection and analysis were performed by Hui Yang, Xin-Yu Zhang, Wei-Guo Gu, Bing Dong, Xue-Zhi Jiang, Wen-Tao Zhou and De-Zhong Wang. The first draft of the manuscript was written by Hui Yang and all authors commented on previous versions of the manuscript. All authors read and approved the final manuscript.

Data availability The data that support the findings of this study are openly available in Science Data Bank at <https://doi.org/10.57760/sciencedb.08126> and <https://cstr.cn/31253.11.sciencedb.08126>

Declarations

Conflict of interest The authors declare that they have no competing interests.

References

1. International Atomic Energy Agency, Classification of Radioactive Waste, IAEA Safety Standards Series No. GSG-1, IAEA, Vienna (2009)
2. International Atomic Energy Agency, Interim Storage of Radioactive Waste Packages, Technical Reports Series No. 390, IAEA, Vienna (1998)
3. International Atomic Energy Agency, *Strategy and Methodology for Radioactive Waste Characterization, IAEA-TECDOC-1537* (IAEA, Vienna, 2007)
4. P. Ormai, A. Fritz, J. Solymosi et al., Inventory determination of low and intermediate level radioactive waste of Paks Nuclear Power Plant origin. *J. Radioanal. Nucl. Chem. Art.* **211**, 443–451 (1996). <https://doi.org/10.1007/BF02039710>
5. M. Kashiwagi, H. Masui, Y. Denda et al., ISO Standardization of the Scaling Factor Method for Low- and Intermediate Level Radioactive Wastes Generated at Nuclear Power Plants. In: 11th International Conference on Environmental Remediation and Radioactive Waste Management, Parts A and B. ASMEDC, pp. 625–629 (2007). <https://doi.org/10.1115/ICEM2007-7015>
6. Standard Guide for Making Quality Nondestructive Assay Measurements, Accessed October 12, 2020. <https://compass.astm.org/download/C1592C1592M-WITHDRAWN.4230.pdf>
7. American Society for Testing and Materials, Standard Test Method for Nondestructive Assay of Special Nuclear Material in Low Density Scrap and Waste by Segmented Passive Gamma-Ray Scanning. https://doi.org/10.1520/C1133_C1133M-10
8. Y.F. Bai, E. Mauerhofer, D.Z. Wang et al., An improved method for the non-destructive characterization of radioactive waste by gamma scanning. *Appl. Radiat. Isot.* **67**, 1897–1903 (2009). <https://doi.org/10.1016/j.apradiso.2009.05.017>
9. Z.L. Cheng, Z. Lu, Z. Huang et al., An improved segmented gamma scanning for radioactive waste drums. *Math. Biosci. Eng.* **16**, 4491–4505 (2010). <https://doi.org/10.3934/mbe.2019224>
10. Y.F. Bai, D.Z. Wang, M. Eric et al., MC simulation of thermal neutron flux of large samples irradiated by 14 MeV neutrons. *Nucl. Sci. Tech.* **21**(1), 11–15 (2010)
11. C. Liu, W.G. Gu, N. Qian et al., Study of image reconstruction using dynamic grids in tomographic gamma scanning. *Nucl. Sci. Tech.* **23**, 277–283 (2012)
12. N. Qian, T. Krings, E. Mauerhofer et al., Analytical calculation of the collimated detector response for the characterization of nuclear waste drums by segmented gamma scanning. *J. Radioanal. Nucl. Chem.* **292**, 1325–1328 (2012). <https://doi.org/10.1007/s10967-011-1601-1>
13. W.G. Gu, C. Liu, N. Qian et al., Study on detection simplification of tomographic gamma scanning using dynamic grids applied in the emission reconstruction. *Ann. Nucl. Energy* **58**, 113–123 (2013). <https://doi.org/10.1016/j.anucene.2013.02.031>
14. Q. Nan, D.Z. Wang, C. Wang et al., Collimated LaBr 3 detector response function in radioactivity analysis of nuclear waste drums. *Nucl. Sci. Tech.* **24**, 060203 (2013). <https://doi.org/10.13538/j.1001-8042/nst.2013.06.006>
15. W. Gu, K. Rao, D. Wang et al., Semi-tomographic gamma scanning technique for non-destructive assay of radioactive waste drums. *IEEE Trans. Nucl. Sci.* **63**, 2793–2800 (2016). <https://doi.org/10.1109/TNS.2016.2614964>
16. W.G. Gu, D.Z. Wang, X.H. Tang et al., An improved gamma scanning assay method for the 400-L compacted radioactive waste drum based on the segmented equivalent ring source. *IEEE Trans. Nucl. Sci.* **66**, 1889–1896 (2019). <https://doi.org/10.1109/TNS.2019.2920180>
17. H. Yang, B. Dong, W.G. Gu et al., Transmission reconstruction algorithm by combining maximum-likelihood expectation

- maximization and a convolutional neural network for radioactive drum characterization. *Appl. Radiat. Isot.* **184**, 110172 (2022). <https://doi.org/10.1016/j.apradiso.2022.110172>
18. H. Yang, H. Zhou, B. Dong et al., A novel transmission reconstruction algorithm for radioactive drum characterization. In: Volume 9: Decontamination and Decommissioning, Radiation Protection, and Waste Management. American Society of Mechanical Engineers, V009T09A005 (2022). <https://doi.org/10.1115/ICONE29-90126>
 19. Office of the Federal Register, National Archives and Records Administration. 10 CFR 61 – Licensing requirements for land disposal of radioactive waste. Code of Federal Regulations, title 10, 153–179 (2016). <https://www.govinfo.gov/app/details/CFR-2006-title10-vol2/CFR-2006-title10-vol2-part61>. Accessed 26 June 2022
 20. International Atomic Energy Agency, Determination and use of scaling factors for waste characterization in nuclear power plants, IAEA Nuclear Energy Series No. NW-T-1.18, IAEA, Vienna (2009)
 21. M.I. Abbas, M.S. Badawi, I.N. Ruskov et al., Calibration of a single hexagonal NaI(Tl) detector using a new numerical method based on the efficiency transfer method. *Nucl. Instrum. Methods Phys. Res. Sect. A* **771**, 110–114 (2015). <https://doi.org/10.1016/j.nima.2014.10.056>
 22. H. Yang, W. Gu, X. Zhang et al., Research on the γ spectrum-unfolding method of low- and intermediate-level radioactive waste based on LaBr₃(Ce) detector. *Radiat. Phys. Chem.* **207**, 110841 (2023). <https://doi.org/10.1016/j.radphyschem.2023.110841>
 23. H. Yang, W. Gu, X. Zhang et al., Research on the CdZnTe γ spectrum analysis method based on an intelligent dynamic library. *J. Radioanal. Nucl. Chem.* **332**, 1847–1867 (2023). <https://doi.org/10.1007/s10967-023-08858-9>
 24. M.W. Rawool-Sullivan, R.J. Estep, D. Miko, Estimation of obliquely scattered gamma-ray response functions in the gross-count tomographic gamma scanner (GC-TGS) method. In: 1997 IEEE Nuclear Science Symposium Conference Record., pp. 774–778 (1997). <https://doi.org/10.1109/NSSMIC.1997.672697>
 25. R. Venkataraman, M. Villani, S. Croft et al., An integrated Tomographic Gamma Scanning system for non-destructive assay of radioactive waste. *Nucl. Instrum. Methods Phys. Res. Sect. A* **579**, 375–379 (2007). <https://doi.org/10.1016/j.nima.2007.04.125>
 26. J.T. Routti, S.G. Prussin, Photopeak method for the computer analysis of gamma-ray spectra from semiconductor detectors. *Nucl. Instrum. Methods.* **72**, 125–142 (1969). [https://doi.org/10.1016/0029-554X\(69\)90148-7](https://doi.org/10.1016/0029-554X(69)90148-7)
 27. H. Cheng, Bao Hua Sun, L.H. Zhu et al., Intrinsic background radiation of LaBr₃(Ce) detector via coincidence measurements and simulations. *Nucl. Sci. Tech.* **31**, 99 (2020). <https://doi.org/10.1007/s41365-020-00812-8>
 28. M.A. Mariscotti, A method for automatic identification of peaks in the presence of background and its application to spectrum analysis. *Nucl. Instrum. Methods.* **50**, 309–320 (1967). [https://doi.org/10.1016/0029-554X\(67\)90058-4](https://doi.org/10.1016/0029-554X(67)90058-4)
 29. INTERNATIONAL ATOMIC ENERGY AGENCY, *Intercomparison of Gamma Ray Analysis Software Packages, IAEA-TEC-DOC-1011* (IAEA, Vienna, 1998)
 30. Canberra. Genie 2000 Operations Manual. <https://www3.nd.edu/~wzech/Genie%202000%20Operations%20Manual.pdf>. Accessed 26 June 2022
 31. I.A. Slavić, S.P. Bingulac, A simple method for full automatic gamma-ray spectra analysis. *Nucl. Instrum. Methods.* **84**, 261–268 (1970). [https://doi.org/10.1016/0029-554X\(70\)90270-3](https://doi.org/10.1016/0029-554X(70)90270-3)
 32. A. Robertson, W.V. Prestwich, T.J. Kennett, An automatic peak-extraction technique. *Nucl. Instrum. Methods.* **100**, 317–324 (1972). [https://doi.org/10.1016/0029-554X\(72\)90701-X](https://doi.org/10.1016/0029-554X(72)90701-X)
 33. I.A. Slavić, Automatic analysis of gamma-ray spectra. *Nucl. Instrum. Methods.* **112**, 253–260 (1973). [https://doi.org/10.1016/0029-554X\(73\)90804-5](https://doi.org/10.1016/0029-554X(73)90804-5)
 34. H.P. Blok, J.C. de Lange, J.W. Schotman, A new peak search method for an automatic spectrum analysis program. *Nucl. Instrum. Methods.* **128**, 545–556 (1975). [https://doi.org/10.1016/0029-554X\(75\)90523-6](https://doi.org/10.1016/0029-554X(75)90523-6)
 35. C.J. Sullivan, S.E. Garner, K.B. Butterfield, Wavelet analysis of gamma-ray spectra. In: IEEE Symposium Conference Record Nuclear Science 2004. 281–286 (2004). <https://doi.org/10.1109/NSSMIC.2004.1462198>
 36. J.W. Wang, W.G. Gu, H. Yang et al., Analytical method for γ energy spectrum of radioactive waste drum based on deep neural network. *Nucl. Tech.* **45**, 53–59 (2022). <https://doi.org/10.11889/j.0253-3219.2022.hjs.45.040501> (in Chinese)
 37. ORTEC. GammaVision Users Manual. <https://manualzz.com/doc/o/nbci8/ortec-gammavision-v7-user-manual-783620h-md-a-preset>. Accessed 18 June 2022
 38. E. Clayton, PIXAN: the Lucas Heights PIXE analysis computer package. AAEC/M--113(1986). ISBN 0 642 59841 X
 39. M. Morháč, An algorithm for determination of peak regions and baseline elimination in spectroscopic data. *Nucl. Instrum. Methods Phys. Res. Sect. A* **600**, 478–487 (2009). <https://doi.org/10.1016/j.nima.2008.11.132>
 40. M.C. Ali Santoro, M.J. Anagnostakis, T. Boshkova et al., Determining the probability of locating peaks using computerized peak-location methods in gamma-ray spectra as a function of the relative peak-area uncertainty. *Appl. Radiat. Isot.* **155**, 108920 (2020). doi:<https://doi.org/10.1016/j.apradiso.2019.108920>
 41. G.F. Knoll, *Radiation Detection and Measurement*, 4th edn. (Wiley, Hoboken, 2010)
 42. International Electrotechnical Commission. IEC 61453:2007 Nuclear instrumentation - Scintillation gamma ray detector systems for the assay of radionuclides—Calibration and routine tests. <https://webstore.iec.ch/publication/5471>. Accessed December 7, 2022
 43. M. Morháč, J. Kliman, V. Matoušek et al., Efficient one- and two-dimensional gold deconvolution and its application to γ -ray spectra decomposition. *Nucl. Instrum. Methods Phys. Res. Sect. A* **401**, 385–408 (1997). [https://doi.org/10.1016/S0168-9002\(97\)01058-9](https://doi.org/10.1016/S0168-9002(97)01058-9)
 44. C.M. Salgado, L.E.B. Brandão, R. Schirru et al., Validation of a NaI(Tl) detector's model developed with MCNP-X code. *Prog. Nucl. Energy.* **59**, 19–25 (2012). <https://doi.org/10.1016/j.pnucene.2012.03.006>
 45. M. Morháč, V. Matoušek, J. Kliman, Optimized multidimensional nonoscillating deconvolution. *J. Comput. Appl. Math.* **140**, 639–658 (2002). [https://doi.org/10.1016/S0377-0427\(01\)00521-0](https://doi.org/10.1016/S0377-0427(01)00521-0)
 46. M. Morháč, Deconvolution methods and their applications in the analysis of γ -ray spectra. *Nucl. Instrum. Methods Phys. Res. Sect. A* **559**, 119–123 (2006). doi:<https://doi.org/10.1016/j.nima.2005.11.129>
 47. R. Gold, An iterative unfolding method for response matrices. United States (1964). <https://doi.org/10.2172/4634295>
 48. M. Morháč, V. Matoušek, High-resolution boosted deconvolution of spectroscopic data. *J. Comput. Appl. Math.* **235**, 1629–1640 (2011). <https://doi.org/10.1016/j.cam.2010.09.005>
 49. S. Steenstrup, A simple procedure for fitting a background to a certain class of measured spectra. *J. Appl. Crystallogr.* **14**, 226–229 (1981). <https://doi.org/10.1107/S0021889881009242>
 50. S.A. Gerasimov, Simple method for background subtraction in gamma-ray spectra. *Int. J. Rad. Appl. Instrum.* **43**, 1529–1531 (1992). [https://doi.org/10.1016/0883-2889\(92\)90186-I](https://doi.org/10.1016/0883-2889(92)90186-I)
 51. C.V. Hampton, B. Lian, W.C. McHarris, Fast-Fourier-transform spectral enhancement techniques for γ -ray spectroscopy. *Nucl.*

- Instrum. Meth. Phys. Res. Sect. A **353**(1–3), 280–284 (1994) [https://doi.org/10.1016/0168-9002\(94\)91657-8](https://doi.org/10.1016/0168-9002(94)91657-8)
52. C.G. Ryan, E. Clayton, W.L. Griffin et al., SNIP, a statistics-sensitive background treatment for the quantitative analysis of PIXE spectra in geoscience applications. *Nucl. Instrum. Meth. Phys. Res. Sect. B* **34**, 396–402 (1988). [https://doi.org/10.1016/0168-583X\(88\)90063-8](https://doi.org/10.1016/0168-583X(88)90063-8)
 53. C.J. Sullivan, M.E. Martinez, S.E. Garner, Wavelet analysis of sodium iodide spectra. *IEEE Nuclear Science Symposium Conference Record*, 2005, Fajardo, PR, USA, 302–306 (2005). <https://doi.org/10.1109/NSSMIC.2005.1596258>
 54. S. Lovejoy, D. Schertzer, Haar wavelets, fluctuations and structure functions: convenient choices for geophysics. *Nonlinear Process. Geophys.* **19**, 513–527 (2012). <https://doi.org/10.5194/npg-19-513-2012>
 55. J.M. Gregoire, D. Dale, R.B. van Dover, A wavelet transform algorithm for peak detection and application to powder x-ray diffraction data. *Rev. Sci. Instrum.* **82**, 015105 (2011). <https://doi.org/10.1063/1.3505103>
 56. J. Uher, G. Roach, J. Tickner, Peak fitting and identification software library for high resolution gamma-ray spectra. *Nucl. Instrum. Methods Phys. Res. Sect. A* **619**, 457–459 (2010). doi:<https://doi.org/10.1016/j.nima.2009.12.086>
 57. A. Likar, A peak-search method based on spectrum convolution. *J. Phys. Appl. Phys.* **36**, 1903–1909 (2003). <https://doi.org/10.1088/0022-3727/36/15/323>
 58. M. Morháč, J. Kliman, V. Matoušek et al., Background elimination methods for multidimensional coincidence γ -ray spectra. *Nucl. Instrum. Methods Phys. Res. Sect. Accel. Spectrometers Detect. Assoc. Equip.* **401**, 113–132 (1997). [https://doi.org/10.1016/S0168-9002\(97\)01023-1](https://doi.org/10.1016/S0168-9002(97)01023-1)
 59. J.L. Coolidge, The story of the binomial theorem. *Am. Math. Mon.* **56**, 147–157 (1949). <https://doi.org/10.1080/00029890.1949.11999350>
 60. M.S. Badawi, A.M. El-Khatib, M.E. Krar, New numerical simulation approach to calibrate the NaI(Tl) detectors array using non-axial extended spherical sources. *J. Instrum.* **8**, P11005 (2013). <https://doi.org/10.1088/1748-0221/8/1/P11005>
 61. M.S. Badawi, M. Abd-Elzaher, A.A. Thabet et al., An empirical formula to calculate the full energy peak efficiency of scintillation detectors. *Appl. Radiat. Isot.* **74**, 46–49 (2013). <https://doi.org/10.1016/j.apradiso.2012.12.011>
 62. Canberra.NDA 2000. <https://www.mirion.com/products/nda-2000-non-destructive-assay-software>. Accessed 15 Nov.2022
 63. American Society for Testing and Materials. ASTM E181–17 Standard Test Methods for Detector Calibration and Analysis of Radionuclides. <https://doi.org/10.1520/E0181-17>
 64. ORTEC. Comparison of Gamma Ray Nondestructive Assay Measurement Techniques. <https://www.ortec-online.com/-/media/amete>
 65. S. Agostinelli, J. Allison, K. Amako et al., Geant4—a simulation toolkit. *Nucl. Instrum. Methods Phys. Res. Sect. Accel. Spectrometers Detect. Assoc. Equip.* **506**, 250–303 (2003). [https://doi.org/10.1016/S0168-9002\(03\)01368-8](https://doi.org/10.1016/S0168-9002(03)01368-8)
 66. W. Tang, J.G. Liang, Y. Ge et al., A method for neutron-induced gamma spectra decomposition analysis based on Geant4 simulation. *Nucl. Sci. Tech.* **33**, 154 (2022). <https://doi.org/10.1007/s41365-022-01144-5>
 67. A.M. El-Khatib, M.S. Badawi, A.A. Thabet et al., Well-type NaI(Tl) detector efficiency using analytical technique and ANGLE 4 software based on radioactive point sources located out the well cavity. *Chin. J. Phys.* **54**, 338–346 (2016). <https://doi.org/10.1016/j.cjph.2016.03.019>
 68. M.T. Haj-Heidari, M.J. Safari, H. Afarideh et al., Method for developing HPGe detector model in Monte Carlo simulation codes. *Radiat. Meas.* **88**, 1–6 (2016). <https://doi.org/10.1016/j.radmeas.2016.02.035>
 69. Y.M. Gómez, H.A.C. Águila, C.M.A. Hernández et al., Monte Carlo simulation of the efficiency response of a well-type HPGe detector at 46.54 keV (2015). <http://scielo.sld.cu/pdf/nuc/n57/nuc015715.pdf> Accessed 28 Jan.2023
 70. M.S. Badawi, S.I. Jovanovic, A.A. Thabet et al., Calibration of 4π NaI(Tl) detectors with coincidence summing correction using new numerical procedure and ANGLE4 software. *AIP Adv.* **7**, 035005 (2017). <https://doi.org/10.1063/1.4978214>
 71. M. Jeřkovský, A. Javorník, R. Breier et al., Experimental and Monte Carlo determination of HPGe detector efficiency. *J. Radioanal. Nucl. Chem.* **322**, 1863–1869 (2019). <https://doi.org/10.1007/s10967-019-06856-4>
 72. American Society for Testing and Materials. American National Standard Calibration and Use of Germanium Spectrometers for the Measurement of Gamma-Ray Emission Rates of Radionuclides. ANSI Std N42.14–1991, pp.1–76, 30 Oct. (1991). <https://doi.org/10.1109/IEEEESTD.1991.101072>
 73. IEEE Standard Test Procedures for Germanium Gamma-Ray Detectors. IEEE Std 325–1996. 0_1- Published online 1997. <https://doi.org/10.1109/IEEEESTD.1997.82400>

Springer Nature or its licensor (e.g. a society or other partner) holds exclusive rights to this article under a publishing agreement with the author(s) or other rightsholder(s); author self-archiving of the accepted manuscript version of this article is solely governed by the terms of such publishing agreement and applicable law.